Pmu1a, a novel spider toxin with dual inhibitory activity at pain targets hNa V 1 .7 and hCa V 3 voltage-gated channels

Julien Giribaldi, Jean Chemin, Marie Tuifua, Jennifer Deuis, Rosanna Mary, Irina Vetter, David Wilson, Norelle Daly, Christina Schroeder, Emmanuel Bourinet, et al.

Dutertre Sebastien (Orcid ID: 0000-0002-2945-1484)

Color : Fig 1-5

Pmu1a, a novel spider toxin with dual inhibitory activity at pain targets hNa$_V$1.7 and hCa$_V$3 voltage-gated channels

Julien Giribaldi[1,2,#], Jean Chemin[3], Marie Tuifua[1], Jennifer R. Deuis[4], Rosanna Mary[1], Irina Vetter[4,5], David T. Wilson[6], Norelle L. Daly[6], Christina I. Schroeder[2,4,#], Emmanuel Bourinet[3], and Sébastien Dutertre[1,*]

[1]IBMM, Université de Montpellier, CNRS, ENSCM, 34095 Montpellier, France.
[2]Center for Cancer Research, National Cancer Institute, National Institutes of Health, Frederick, MD, 21702, USA.
[3]Institute of Functional Genomics, Montpellier University, CNRS, INSERM, Montpellier, France.
[4]Institute for Molecular Bioscience, The University of Queensland, Brisbane, Qld, 4072, Australia.
[5]School of Pharmacy, The University of Queensland, Woolloongabba, Qld, 4102, Australia.
[6]Centre for Molecular Therapeutics, Australian Institute of Tropical Health and Medicine, James Cook University, Cairns, QLD, Australia.

[*] Corresponding author: sebastien.dutertre@umontpellier.fr
[#] Current address: Genentech, 1 DNA Way, South San Francisco, CA, 94080, USA

Running title: Pmu1a blocks both hNa$_V$1.7 and hCa$_V$3 channels

Abbreviations: ICK, inhibitor cystine knot; NMR, nuclear magnetic resonance; IPA, isopropyl alcohol; ACN, acetonitrile; HEK, human embryonic kidney; RP-HPLC, reverse-phase high performance liquid chromatography; RMSD, root-mean-square deviation; LVA, low-voltage activated; CHO, chinese hamster ovary; LC/MS, liquid chromatography coupled mass spectrometry

Keywords: Spider peptide, voltage-gated calcium channel, voltage-gated sodium channel, dual activity, inhibitory cystine knot

Conflicts of interest: JC, MT, JRD, RM, IV, DW, NLD, EB, and SD declare that they have no conflicts of interest with the contents of this article. JG and CIS are employees of Genentech, Inc. and shareholders of Roche.

This article has been accepted for publication and undergone full peer review but has not been through the copyediting, typesetting, pagination and proofreading process which may lead to differences between this version and the Version of Record. Please cite this article as doi: 10.1111/febs.16773

ABSTRACT

Venom-derived peptides targeting ion channels involved in pain are regarded as a promising alternative to current, and often ineffective, chronic pain treatments. Many peptide toxins are known to specifically and potently block established therapeutic targets, among which the voltage-gated sodium and calcium channels are major contributors. Here, we report on the discovery and characterization of a novel spider toxin isolated from the crude venom of *Pterinochilus murinus* that shows inhibitory activity at both $hNa_V1.7$ and $hCa_V3.2$ channels, two therapeutic targets implicated in pain pathways. Bioassay-guided HPLC fractionation revealed a 36-amino acid peptide with three disulfide bridges named μ/ω-theraphotoxin-Pmu1a (Pmu1a). Following isolation and characterization, the toxin was chemically synthesized, and its biological activity was further assessed using electrophysiology, revealing Pmu1a to be a toxin that potently blocks both $hNa_V1.7$ and hCa_V3. NMR structure determination of Pmu1a shows an inhibitor cystine knot (ICK) fold that is characteristic of many spider peptides. Combined, these data show the potential of Pmu1a as a basis for the design of compounds with dual activity at the therapeutically relevant $hCa_V3.2$ and $hNa_V1.7$ voltage-gated channels.

Introduction

Currently, more than 30% of the world's population suffers from chronic pain [1]. Despite being widely studied, chronic pain management has changed little over the last decades and remains highly reliant on opioid treatment, resulting in inadequate pain relief, side effects and addiction manifesting itself in an opioid crisis sweeping across the United States [2,3]. Collectively, this strongly advocates the development of effective and safe non-opioid pain treatments.

Animal venoms represent an important source of bioactive molecules, including peptide toxins, evolved to incapacitate preys or to fight off aggressors/predators [4–6]. Over the last three decades, technological advances including improved analytical techniques and high-throughput screening in combination with the emergence of omics approaches have greatly expanded the knowledge around venoms [5,7]. Several drugs have been developed from the venom of different species, including lizards, snakes and cone snails for a variety of conditions such as diabetes, hypertension, hemostasis control and chronic pain [4,5].

Voltage-gated sodium channels are key in the initiation and propagation of nerve action potentials, and the $Na_V1.7$ isoform has been implicated to play an important role in pain pathways [8]. Genetic evidence has shown that mutations in the SCN9A gene, that encodes for the $Na_V1.7$ sodium channel subtype, cause pain-related pathologies [9,10]. Several spider-derived venom peptides have displayed high affinity and selectivity for $Na_V1.7$ subtypes including Gr2a, Hh2a and Tp2a [11]. Recently, μ-theraphotoxin-Pn3a, isolated from the venom of *Pamphobeteus nigricolor* was characterized as a $Na_V1.7$ sodium channel inhibitor. Interestingly, a recent study demonstrated that Pn3a also inhibited Ca_V1 and Ca_V2 subtype family as well as $Ca_V3.3$ channels at high concentrations [12,13]. Interestingly, when administered in combination with subtherapeutic doses of opioids, the Pn3a peptide can produce profound analgesic activity in inflammatory animal models [14]. Another spider toxin, μ-theraphotoxin-Pspp1, also known as phlotoxin 1 (PhlTx1) from the spider venom of a *Phlogiellus sp*., has been shown to inhibit $Na_V1.7$ in mammalian cells expressing this sodium channel subtype. Furthermore, this peptide toxin was able to reduce pain-like responses in mouse models of inflammatory pain [15]. Together, these results suggest that spider toxins targeting voltage-gated sodium channels could have potential for the treatment of pain.

The mechanisms underlying the development of pain are complex and in addition to sodium channel subtypes, including $Na_V1.7$, numerous studies have also revealed the implication of neuronal voltage-gated calcium channels [16,17]. ω-Conotoxin-MVIIA, isolated from *Conus magus*, and inhibits N-type $Ca_V2.2$, was FDA approved in 2004 for the treatment of severe chronic pain [18]. In addition, ω-conotoxin-GVIA and ω-conotoxin-CVID isolated from *C. geographus* and *C. catus* species, respectively, which also target $Ca_V2.2$, have demonstrated analgesic properties *in vivo* [19,20]. One limitation of targeting $Ca_V2.2$ as an analgesic target is the necessity for intrathecal administration to specifically target spinal sites and limit the side effects [21]. Further characterization of pain pathways has also implicated T-type calcium channels (Ca_V3) in nociceptive transmission [22,23]. Activated by very low depolarization near resting membrane

potentials and located in the cell membrane, they control neuronal excitability and participate in many calcium-dependent functions including neuronal firing, hormone secretion, smooth muscle contraction, myoblast fusion, and fertilization [24]. In opposition to $Ca_V2.2$ subtypes, Ca_V3 are peripherally accessible, which make them promising putative analgesic targets [25]. Administration of T-type calcium channel inhibitors, including mibefradil, ethosuximide, or more recently developed selective pan-T-type blockers such as TTA-A2 and Z944 produced analgesic effects in animal models [26–29]. Among T-type channels, the isoform $Ca_V3.2$ is largely expressed in primary sensory neurons [30], thus suggesting a role in the nociceptive mechanism. Importantly, in mice, the $Ca_V3.2$ calcium channel is a selective marker of the Aδ- and C- low-threshold mechanoreceptors (LTMRs) involved in the pathophysiology of chronic pain models [31,32]. One *in vivo* study in mononeuropathic rats showed silencing of the $Ca_V3.2$ gene by antisense oligodeoxynucleotides caused antinociceptive, antihyperalgesic and anti-allodynic effects [33]. Similarly, in a rat model of irritable bowel syndrome, $Ca_V3.2$ channels contributed to the exaggerated colonic hypersensitivity [34]. These results suggest that the $Ca_V3.2$ voltage-gated calcium channel is a potential analgesic target for future therapeutic pain management approaches.

In this study, we report the identification and characterizations of μ/ω-theraphotoxin-Pmu1a [35] (Pmu1a), a 36-amino acid peptide isolated from the venom of the tarantula *Pterinochilus murinus*. Initial bioassay-guided HPLC fractionation showed potent inhibitory activity of *P. murinus* crude venom on $hCa_V3.2$ voltage-gated channels. Further electrophysiological studies using synthetic material revealed inhibitory activity of Pmu1a on both $hCa_V3.2$ and $hNa_V1.7$ and allowed its pharmacological characterization on additional subtypes of hNa_V and hCa_V3 channels. These results suggest that Pmu1a is a novel voltage-gated ion channel inhibitor that may provide a basis for the development of novel agents with dual pharmacology.

Results

Screening of Pterinochilus murinus crude venom against $hCa_V3.2$ voltage-gated channels and isolation of Pmu1a

Venom from the spider species *Pterinochilus murinus* (1 mg/mL) inhibited 50% of the current using manual whole-cell patch clamp electrophysiology in HEK293 cells overexpressing $hCa_V3.2$ (data not shown). The crude venom of *P. murinus* was fractionated using RP-HPLC and individual fractions were evaluated for activity using manual whole-cell patch clamp electrophysiology in HEK293 cells overexpressing $hCa_V3.2$. Fraction 32 (Figure 1A) of *P. murinus* inhibited $hCa_V3.2$ calcium channels by reducing the current by more than 80% (data not shown). Further purification of fraction 32 (Figure 1B) revealed that sub-fraction 32.6 effectively inhibited more than 90% of $hCa_V3.2$ current in HEK293 cells overexpressing $hCa_V3.2$ (Figure 1C). Mass spectrometry analysis determined that the dominant peak in sub-fraction 32.6 displayed a monoisotopic mass of 4350.83 Da (Figure 1D). Edman degradation revealed a 36-amino acid toxin containing six cysteines, which was named Pmu1a, according to the current nomenclature [35] (Figure 2). Due to limited quantity of native material, the disulfide connectivity could not be

determined experimentally. However, the primary amino acid sequence follows the consensus described for inhibitor cystine knot (ICK) framework: $CX_{3-7}CX_{3-6}CX_{0-5}CX_{1-4}CX_{4-13}C$, where X can be any amino acid [36]. This particular motif, found in many spider-venom peptides, comprises a ring formed by two disulfides and the intervening sections of polypeptide backbone, with a third disulfide piercing the ring to create a pseudo-knot [37].

This is the first toxin described so far from the crude venom of the spider *P. murinus*, known as the "orange baboon tarantula", a member of the Theraphosidae spider family. A BLAST search revealed that the closest relatives were a group of uncharacterized sequences from the spider *Grammostola rosea* (percentage identity ranging from 75 to 77 %). However, Pn3a from *Pamphobeteus nigricolor* is the most similar peptide (58% sequence identity) for which pharmacological and structural characterizations were available (Figure 2).

Chemical synthesis of Pmu1a

The quantity of native peptide isolated from the crude venom was not sufficient to perform additional bioassays and structure determination, therefore, the peptide was chemically synthesized using automated Fmoc-SPPS [38] with a yield of 10% for the pure linear peptide. When screening for optimum folding conditions, we found that using NH_4OAc as a basic buffer and guanidine hydrochloride (GnHCl) as a denaturant promoted the formation of one major isomer (Figure 3A). Replacing GnHCl by urea in the oxidation buffer further increased the formation of the major isomer as evidenced by the relative increase in peak area (Figure 3B). Additionally, due to decreased solubility of the peptide during oxidation, as suggested by the diminishing peak area over time (Figure 3B), isopropyl alcohol (IPA) and acetonitrile (ACN) were evaluated as co-solvent. The addition of IPA did not promote the formation of the desired isomer (data not shown) but the use of 50% ACN improved the oxidation yield compared to conditions without ACN (Figure 3C). Following optimization of the folding conditions, NH_4OAc containing 1.475 M urea and 50% ACN were used. The synthetic peptide was isolated with 12% yield (Figure 3D) from pure linear peptide and co-eluted with the native peptide (data not shown). Interestingly, when the purified peptide was solubilized after lyophilization, an additional minor peak was present in the RP-HPLC chromatogram (Figure 3D). Isolation of the main peak followed by a second round of RP-HPLC purification led to the same RP-HPLC chromatogram profile containing an additional small peak, suggesting that the peptide undergoes dynamic conformational exchange to a small extent.

Activity of synthetic Pmu1a at voltage- and ligand-gated ion channels using electrophysiology and calcium fluorescence imaging

Synthetic Pmu1a was evaluated for activity at $hCa_V3.2$ overexpressed in HEK293 cells using manual whole-cell patch clamp electrophysiology, displaying an IC_{50} of 955.4 $\pm$ 235.5 nM (Figure 4A, table 1). Because of the sequence similarity between Pmu1a and Pn3a, a selective $Na_V1.7$ inhibitor, synthetic Pmu1a was also evaluated for activity against a panel of voltage-gated sodium channels overexpressed in HEK293 cells, including $hNa_V1.7$, $hNa_V1.6$ and $hNa_V1.4$, using automated whole-cell patch clamp electrophysiology experiments. Pmu1a inhibited $hNa_V1.7$ and $hNa_V1.6$ channels with high potency ($Na_V1.7$ IC_{50} 7.0 $\pm$ 0.7 nM, $Na_V1.6$ IC_{50} 9.9 $\pm$ 1.7 nM) and

hNa$_V$1.4 with ~8-fold lower potency (IC_{50} 62.9 ± 8.1 nM) (Figure 4B, table 1). Inhibition of hNa$_V$1.7 was further confirmed by manual whole-cell patch clamp electrophysiology, where Pmu1a displayed an IC_{50} value of 5.5 ± 0.4 nM (Figure 4A). Although the original screening campaign was performed on hCa$_V$3.2 channels, the selectivity profile of Pmu1a on all three subtypes of Ca$_V$3 channels was further investigated using manual whole-cell patch clamp electrophysiology. Interestingly when tested at 10 µM, Pmu1a inhibits 95.1 ± 0.6 % (n=4) of hCa$_V$3.1 current, 90.8 % ± 1.5 % (n=4) of hCa$_V$3.3 and 63.5 ± 4.7 % (n=6) of hCa$_V$3.2 current (Figure 4C, table 1). Pmu1a also induced a strong rightward shift in the current-voltage curves of hCa$_V$3 currents. The $V_{1/2}$ values in the absence and in the presence of toxin, for hCa$_V$3.1, hCa$_V$3.2, hCa$_V$3.3 current-voltage curves were −43.1 ± 0.9 and −21.7 ± 3.4 mV ($p<0.01$, n=4), −48.8 ± 2.6 and −37.2 ± 1.3 mV ($p<0.05$, n=3), −45.4 ± 1.1 and −19.3 ± 2.6 mV ($p<0.01$, n=4) respectively. This strong shift in the current-voltage curves might suggest that PmuTx1 could act as a gating modifier of Ca$_V$3 currents. To further test this hypothesis, we investigated the effect of the toxin at very positive voltage (+100 mV), for which Ca$_V$3 currents are fully activated. (Figure 4E). We found that 10 µM PmuTx1 has no inhibitory effect on Ca$_V$3.1 (n=6) and Ca$_V$3.3 (n=4) currents elicited at +100 mV whereas Ca$_V$3.2 were inhibited by less than 15 % (n=5). On the contrary, in these experiments PmuTx1 induced ~86 % inhibition of Ca$_V$3.1 current, ~53 % inhibition of Ca$_V$3.2 current and ~89 % inhibition of Ca$_V$3.3 current recorded at − 30 mV. Overall, these results suggest that PmuTx1 induced inhibition of Ca$_V$3 currents mainly by inducing a strong depolarizing shift in the current-voltage curve.

Solution structure of synthetic Pmu1a

Two-dimensional (2D) homonuclear NMR spectroscopy was used to determine the three-dimensional (3D) structure of the Pmu1a peptide. Structure calculations were run without disulfide bond restraints and the most likely bond was between Cys2-Cys16 (C1-C4). The connectivity of the remaining disulfide bonds was ambiguous. However, structures were also run with the 15 different possible disulfide connectivities and the lowest target function [39] value was obtained for the C1-C4, C2-C5 and C3-C6 connectivity, suggesting that is the most likely connectivity. The structure was well-defined over residues 4–28 (0.35 ± 0.09 Å RMSD over backbone atoms, Table 2, Figure 5A), but displays a disordered C-terminal across residues 29–36. The final 20 lowest-energy structures were calculated including disulfide constraints. The ensemble superimposes with a low RMSD (0.35 ± 0.09 Å) over backbone atoms of residues 4–28 (Table 2, Figure 5A). Moreover, Pmu1a comprised two antiparallel β-strands, which is typical of the inhibitory cystine knot (ICK) motif characteristic of spider ICK peptides targeting Na$_V$ channels [40] (Figure 5B). The molecular surface clearly indicates an amphipathic peptide where charged residues are mainly on one face (Figure 5C) and hydrophobic residues on the other face of the peptide (Figure 5D). As expected from the amino acid sequence similarity with Pn3a, superimposition of the two peptides over the backbone atoms of residues 1–27 highlight the structural similarity (RMSD value of 0.715 Å (Figure 5B). Despite the presence of a second conformer in the RP-HPLC data, there was no evidence of a second conformer in the NMR spectra, consistent with the low percentage of the second conformer in the chromatographic analysis.

Discussion

Inhibitors for various subtypes of Ca_V channels have been isolated from spider venom [40]. However, spider peptides with activity at T-type Ca_V channels are comparatively rare [41] and low nanomolar inhibitors have not yet been reported for $Ca_V3.2$. $Ca_V3.2$ channels are characterized by their hyperpolarized voltage-activation range and window current, which make them ideally suited to regulate neuronal excitability [25]. They are expressed in various subpopulations of primary afferent neurons. Furthermore, knockdown and channel blockade mediate analgesia[25]. The majority of Ca_V active spider peptides have shown activity across Ca_V1, $Ca_V2.1$, $Ca_V2.2$ and $Ca_V2.3$ [42–56], with a recent report of the tarantula toxin ω-Avsp1a inhibiting T-type calcium channels $Ca_V3.1$ and $Ca_V3.3$, albeit with low affinity [57]. Recently, low potency inhibition of calcium channels $Ca_V3.3$ by the spider toxin Pn3a, a low nanomolar inhibitor of $Na_V1.7$ sodium channels, was reported [13]. However, the authors did not observe $Ca_V3.2$ inhibition up to 10 μM [13]. Tap1a isolated from *Theraphosa apophysis* venom is thus far the spider toxin displaying the strongest activity on $Ca_V3.2$ channels (IC_{50} 1.2 μM) [41]. The role of $Ca_V3.2$ T-type calcium channels in the nociceptive pathway is still awaiting the discovery and pharmacological elucidation of a selective blocker of $Ca_V3.2$. In this study, Pmu1a, a novel T-type Ca_V3 channels inhibitor, was identified and isolated from *P. murinus* venom.

Identification and initial characterization of Pmu1a was followed by solid-phase peptide synthesis and thermodynamic oxidative folding to obtain material for assays and NMR structure determination. During oxidation of the peptide, urea promoted the more efficient formation of a major folding isomer than guanidine hydrochloride (Figure 3A, B). Addition of urea to the oxidation buffer has previously been used in the folding of the spider peptide Hsp1a and most likely improves oxidation yield by decreasing aggregation [58]. Similarly, the presence of urea was required for solubility of linear Pmu1a, most likely because of the peptide's tendency to aggregate via hydrophobic interactions during the folding reaction. Hydrogen exchange experiments have demonstrated that urea forms hydrogen bonds to peptide NH and CO groups [59], which may promote reduced aggregation leading to higher oxidation yield. For Pmu1a, addition of ACN to the folding buffer further improved solubility and increased the folding yield further (Figure 3C). One explanation could be that one or more key folding intermediates are more soluble in ACN resulting in improved overall yield. The optimized folding conditions provided sufficient material (12% folding yield) to perform bioassays on different subtypes of sodium voltage-gated ion channels and NMR structure determination.

Synthetic Pmu1a inhibits $Ca_V3.2$ (Figure 4A) with submicromolar potency (955.4 nM). To further assess the selectivity profile of Pmua1, we performed additional electrophysiology experiments on other Ca_V3 channels (Figures 4C, D). Interestingly, Pmu1a appears even more potent on $Ca_V3.1$ and $Ca_V3.3$ channels which are also targets with potential therapeutic value. Knock-out of $Ca_V3.1$ channels in rodent shows no low-voltage activated (LVA) Ca^{2+} current in thalamocortical relay neurons with no burst-firing activity [60] as well as decreased mechanical hypersensitivity [61]. Additionally, spike-and-wave discharges were prevented in the absence epilepsy model, and in a model of tonic-clonic generalized seizures, animals were less prone to tonic seizures in the

maximal electroshock seizure test compared to $Ca_V3.2$ knock-outs [62,63]. Loss of LVA Ca^{2+} currents in the thalamic reticular nucleus (nRT) neurons was observed when $Ca_V3.3$ were inactivated in mice suggesting a role in sleep behaviour [64]. The incomplete block of the $Ca_V3.2$ channel (Figure 4A) could indicate either a partial occlusion of the pore or an effect on channel gating [65]. However, the depolarizing shifts observed in the voltage-dependence of activation for $Ca_V3.1$, $Ca_V3.2$, $Ca_V3.3$ (Figure 4D) suggest that Pmu1a acts as a gating modifier of Ca_V3 channels [65]. Accordingly, we found that Pmu1a inhibited all Cav3 currents at -30 mV but had negligible effect at very depolarizing voltage (i.e. +100 mV) (Figure 4E).

Because of the sequence similarity between Pmu1a and Pn3a (Figure 2), activity at $Na_V1.7$ and other subtypes of Na_V channels was also investigated to establish a more complete pharmacological profile. Pmu1a also inhibits $Na_V1.7$ and $Na_V1.6$ with similar potency (5-10 nM) as well as $Na_V1.4$ with ~10-fold less potency compared to $hNa_V1.7$ (Figure 4B). The activity of Pmu1a at the skeletal muscle isoform $Na_V1.4$ and the neuronal isoform $Na_V1.6$ would most likely cause dose-limiting side effects which limits suitability of Pmu1a as an analgesic lead [66,67]. However, Pmu1a is the most potent spider peptide targeting the $Ca_V3.2$ subtype described so far, therefore providing a valuable lead to design a potential potent dual-acting inhibitor.

Despite the sequence similarity between Pmu1a and Pn3a, the two peptides display quite different pharmacological profiles. Therefore, we were interested in investigating the structural differences between Pmu1a and Pn3a. The three-dimensional structure of synthetic Pmu1a was determined using homonuclear solution ^1H NMR. Structure calculations were run with the 15 different possible disulfide connectivities and the lowest target function value was obtained for the C1-C4, C2-C5 and C3-C6 connectivity. Additionally, a strong sequence homology with Pn3a and the ICK scaffold $CX_{3-7}CX_{3-6}CX_{0-5}CX_{1-4}CX_{4-13}C$ [36] of Pmu1a strongly suggests the ICK connectivity. The NMR structure calculated with the ICK disulfide connectivity as a constraint [40] displays a typical ICK topology with two beta strands from L19 to C21 and from C29 to W31. The three-dimensional structures of Pn3a and Pmu1a superimpose well (RMSD 0.715 Å) over backbone atoms (C, CO, N), and the residues important for Pn3a activity at $Na_V1.7$ (Y4, K22, K24, W30) [68] are conserved in the Pmu1a peptide, which could explain the retention of activity for Pmu1a at $Na_V1.7$ (Figure 5B, 4B). Overall, Pmu1a has a conserved amphipathic surface with a hydrophobic patch surrounded by charged residues. One face of the peptide is primarily composed of charged residues (Figure 5C), and the other face is mainly populated by hydrophobic residues (Figure 5D). Interestingly, this surface arrangement is very similar to Pn3a and has been suggested to permit interactions with the membrane and with parts of the voltage-sensing domains located on the extracellular surface [68]. Molecular modeling studies of Pn3a suggests that K22 and K24 strongly interact with the S3-S4 loop of domain II of $Na_V1.7$ while removal of hydrophobic residues Y4, Y27, W30 led to a loss of potency (>250 fold) [68]. In addition, Mueller *et al*. also showed that negatively charged residues E10 and E13 are crucial for selectivity since their substitution with positively charged lysine led to a loss of selectivity between $Na_V1.6$ and $Na_V1.7$ [68]. In contrast, the absence of a negative charge on the equivalent residues in Pmu1a (N10, A13) could explain the lack of selectivity of this peptide for $Na_V1.7$ over $Na_V1.6$ (Figure 4B).

The pharmacology of Pmu1a suggests potential to be used as an analgesic with dual activity at $Na_V1.7$ and Ca_V3 channels including $Ca_V3.2$. Previously when Pn3a failed to produce analgesia *in vivo*, a combination of the peptide with a subtherapeutic dose of opioid was successful [14]. This indicates that combination therapies or dual-acting peptides are worth pursuing. Whereas Pn3a has not yet been established as a dual inhibitor of other pain-relevant voltage-gated ion channels, a recent study demonstrated that the peptide inhibits $Ca_V3.3$ with low potency [13]. However, the implication of this target in the nociceptive pathway is less supported in the literature [64,69]. Tap1a is yet another example of peptide targeting several channels including $Na_V1.1$, $Na_V1.3$, $Na_V1.7$–$Na_V1.9$, $Ca_V2.2$, and $Ca_V3.2$. Tap1a nearly ablated neuronal mechanosensitivity in afferent fibers innervating the colon and the bladder. Additionally, *in vivo* intracolonic administration reversed colonic mechanical hypersensitivity in a mouse model of irritable bowel syndrome [41]. This could have been a result of Tap1a interacting with more than one pain-relevant voltage-gated ion channel. Therefore, Pmu1a's dual inhibition of $Na_V1.7$ and $Ca_V3.2$, two therapeutic targets known to be implicated in pain pathways, might lead to insights into the development of promising non-opioid analgesic peptides.

In summary, Pmu1a is the first peptide isolated from *P. murinus* venom and is a dual inhibitor of Ca_V3 calcium channels, including $Ca_V3.2$, and $Na_V1.7$ sodium channels. However, the low selectivity of Pmu1a for $Na_V1.7$ over $Na_V1.6$ and $Na_V1.4$ and its relatively weak affinity for $Ca_V3.2$ limits its potential use as analgesic without side-effect. Nevertheless, Pmu1a is the most potent spider toxin inhibitor of $Ca_V3.2$ calcium channels described to date. It would be of interest to engineer this peptide further to achieve a low nanomolar potency on $Ca_V3.2$ and $Na_V1.7$ channels while limiting its activity on the skeletal muscle isoform $Na_V1.4$ and the neuronal isoform $Na_V1.6$ for the design of non-opioid analgesic peptide drugs.

Materials and methods

Pterinochilus murinus crude venom screening on $Ca_V3.2$ using whole cell patch clamp electrophysiology

Pterinochilus murinus venom was purchased from a private collector based in France, collected by chelicerae electrostimulation and lyophilized. Venom was evaluated for activity at 1 mg/mL using manual whole-cell patch clamp on HEK293 cells stably overexpressing $Ca_V3.2$ (see protocol below).

Cell culture for manual whole-cell patch clamp electrophysiology

HEK293 cells stably overexpressing $Ca_V3.2$, $Ca_V3.3$ human calcium channels were cultured in T75 flasks with vented caps, at 37 °C with 5% carbon dioxide (CO_2). Cells were cultured in Dulbecco's Modified Eagle's Medium (DMEM, Fisher Scientific) supplemented with 10% of fetal bovine serum (FBS, Gibco, Life technologies) and penicillin and streptomycin antibiotics (Gibco, Life technologies). Geneticin G418 (Gibco, Life technologies) at 300 µg/mL was added to the cells once a week for selection. The CHO cells stably expressing $Ca_V3.1$ human calcium channels were

cultured in T75 flasks with vented caps, at 37 °C with 5% carbon dioxide (CO2). Cells were cultured in α-MEM (Fisher Scientific) supplemented with 10% of Fetal Bovine Serum (FBS), 1 mM pyruvate, penicillin and streptomycin antibiotics (Gibco, Life technologies). Hygromycin was added to the cells at 300 µg/ml once a week for selection.
The CHO cells stably expressing $Na_V1.7$ sodium channels were cultured in T75 flasks with vented caps, at 37 °C with 5% carbon dioxide (CO_2). Cells were cultured in Dulbecco's Modified Eagle's Medium-F12 (DMEM-F12, Fisher Scientific) supplemented with 10% of Fetal Bovine Serum (FBS), 1 mM pyruvate, penicillin and streptomycin antibiotics (Gibco, Life technologies). Hygromycin was added to the cells at 200 µg/mL once a week for selection.

Cells were split twice a week (1:10) upon reaching 80% confluency. Dulbecco's Phosphate Buffer Saline (DPBS, Thermo Fisher Scientific) was used to wash the cells and Versene (ThermoFisher Scientific) to detach the cells. For manual whole-cell patch clamp of *P. murinus* venom fractions on HEK293 cells stably overexpressing $Ca_V3.2$, cells were cultured on coverslips in 35 x 10 mm petri dishes. Before seeding, coverslips were incubated with polyornithine (P.L.O-1X, Fisher scientific) and washed two times with PBS-1X (Gilbo, Life technologies). For manual whole-cell patch clamp of synthetic Pmu1a on HEK293 cells stably overexpressing $Ca_V3.2$, cells were cultured on 35x23 mm Fluorodish cell culture dishes (World Precision Instruments). Cells were also maintained at 37 °C with 5% of CO2.

Manual whole-cell patch-clamp electrophysiology

All electrophysiological experiments were performed at room temperature (20 °C) in a whole-cell patch-clamp configuration at a holding potential of −85 mV for CHO cells expressing $Na_V1.7$, −80 mV for CHO cells expressing $Ca_V3.1$ and HEK293 cells stably overexpressing $Ca_V3.2$, and $Ca_V3.3$. Patch pipettes were made from borosilicate glass (World Precisions Instruments) and had tip resistances of 2–3 MΩ when filled with intracellular solution (ICS) containing 140 mM CsCl, 10 mM HEPES, 10 mM EGTA, 3 mM $CaCl_2$, 3 mM MgATP, and 0.6 mM Na-GTP. Cells were maintained in a bath with extracellular solution (ECS) composed with 135 mM NaCl, 20 mM TEACl, 10 mM HEPES, 4 mM KCl, 1 mM $MgCl_2$, 2 mM $CaCl_2$. pH for both solutions was adjusted at 7.3 with NaOH (adjusted to 320 mOsm/L with sucrose). Currents were recorded with Axopatch 200B amplifier (Axon Instruments) and pClamp10 softwares. Results were analysed with Clampfit 10.7 and GraphPad Prism 8.4.2 software. hCa_V3 currents were elicited by a series of step depolarizations (180 ms duration for Cav3.1 and Cav3.2, and 450 ms duration for Cav3.3) ranging from −80 to +50 mV (0.2 Hz) from a holding potential of −90 mV and by a 10 ms test pulse to 0 mv from a holding potential of −85 mV for $Na_V1.7$ channels (repetition intervals 2 s). Crude venoms were dissolved at 1 mg/mL with extracellular solution supplemented with 0.1% BSA and applied to the cell patched by home-made gravity driven perfusion device after stabilisation of the current. The percentage of inhibition was established by plotting the peak amplitude of the currents recorded from eight cells before and after toxin application. The peak amplitude value obtained after toxin application was multiplied by 100 and divided by the peak amplitude value obtained before toxin application. The result was subtracted from 100 giving the percentage of inhibition. Current–voltage curves were fitted using a combined Boltzmann and linear Ohmic relationships, where $I=Gmax\times(Vm-Vrev)/(1+\exp((Vm-V0.5)/\text{slope factor}))$.

Isolation and purification of Pmu1a

Crude venom (5 mg) was fractionated by RP-HPLC (UltiMate® 3000 Standard LC systems, ThermoFisher Scientific) using a C18 column (Synchronis C_{18}, 254 × 4.6 mm, 5 µm, ThermoScientific) and a gradient of water/acetonitrile (ACN) in 0.1% formic acid from 0−100% over 100 min. The flow rate was 1mL/min and fractions were collected by time in a 96-well plate and lyophilized.

Activity of crude venom fractions on whole cell patch clamp electrophysiology

P. murinus lyophilized fractions were dissolved in 100 µL of extracellular solution supplemented with 0.1% BSA and tested using manual whole-cell patch clamp on HEK293 cells stably overexpressing $Ca_V3.2$ (see protocol above). Fraction 32 was re-purified by RP-HPLC (UltiMate® 3000 Standard LC systems, ThermoFisher Scientific) on a C18 column (Synchronis C_{18}, 254 × 4.6mm, 5 µm, ThermoScientific) using a gradient of water/ACN in 0.1% formic acid from 20−40% ACN over 20 min. Fractions were collected manually. Sub-fraction 32.6 was evaluated for activity using manual whole-cell patch clamp on HEK293 cells stably overexpressing $Ca_V3.2$ (see protocol below) and analyzed by LC-HRMS (Acquity H-Class, Waters, Synapt G2-S, Waters) using a Kinetex C18 100 Å column (100 × 2.1 mm, 2.6 µm particle size) from Phenomenex (France) and a gradient of water/ACN in 0.1% formic acid from 20−40% ACN over 20 min. Peptide mass was determined using electrospray ionization time-of-flight (ESI-TOF) mass spectrometry (Acquity H-Class, Waters, Synapt G2-S, Waters), and the amino acid sequence of the peptide was determined by Edman degradation.

Chemical synthesis of linear Pmu1a

N,N'-dimethylformamide (DMF), N,N diisopropylethylamine (DIPEA), acetonitrile (ACN), triisopropylsilane (TIS), trifluoroacetic acid (TFA), piperidine, N,N'-diisopropylcarbodiimide (DIC), 2,2'-(ethylenedioxy)diethanethiol (DODT) and all other reagents were obtained from Sigma-Aldrich (Saint-Louis, MI, USA) or Chem-Impex International (Wood Dale, IL, USA) and were used as supplied. Fmoc (L) amino acid derivatives, Oxyma Pure and Cl-TCP(Cl) Protide resin (100–200 mesh, 0.4 mmol/g) were purchased from CEM (Matthews, NC, USA). The following sidechain protecting groups were used: Asn/Cys (Trt), Thr/Glu (tBu), Trp/Lys/His (Boc), Asp (OMpe), and Arg (Pbf). Resin loading and Fmoc-SPPS of linear Pmu1a were carried out using a CEM liberty prime microwave peptide synthesizer. Oxyma was prepared at 0.25 M in DMF containing 0.1 M DIPEA. The DIC solution was prepared at 2 M in DMF. Fmoc-Thr(tBu)-OH (2 mL, 0.5 M) was loaded onto 0.1 mmol of resin by adding 2 mL of a KI/DIPEA solution in DMF (0.52 g KI, 4.35 mL DIPEA completed to 25 mL with DMF) 2 x 10 min at 60 °C. Fmoc deprotection was carried out with pyrrolidine (25% in DMF v/v), 2 x 3 min at 60 °C. Subsequent amino acids were coupled twice for 10 min at 60 °C using an amino acid/DIC/Oxyma ratio of 5:10:5 relative to resin loading. Sidechain deprotection and cleavage from the resin was carried out by treating the dried peptide-resin with 10 mL of TFA/TIS/thioanisole/H_2O/DODT (92:2:2:2:2 v/v), 2 x 90 min. The cleavage solution was collected in a round bottom flask and evaporated under vacuum, crude peptide was precipitated

using cold diethyl ether, resolubilized in H_2O/ACN (70:30 v/v) containing 0.1% TFA and stirred overnight.

RP-HPLC Purification of synthetic peptides

Crude synthetic linear peptide was purified by preparative RP-HPLC on a Shimadzu LC-20AT (Kyoto, JPN) system using a preparative column (C18 Jupiter®, 300 Å, 250 x 21.2 mm, 5 µm particle size) and a flow rate of 8 mL/min. Semi preparative RP-HPLC was run on a Shimadzu LC-20AT (Kyoto, JPN) system using a preparative column (NX-C18 Gemini®, 110 Å, 250 x 10 mm, 5 µm particle size) and a flow rate of 3 mL/min. Solvent A was 0.05% TFA in MilliQ water and solvent B was 0.045% TFA in 90% ACN/10% MilliQ water. The purification gradient was from 0–60%B over 60 min and the purification was monitored at 214 and 280 nm. Fractions were collected using a fraction collector (Shimadzu FRC-10A), mass determined by ESI-MS and fractions of interest were lyophilized and stored at −2 °C prior to use.

Thermodynamic folding of synthetic linear Pmu1a

Purified linear Pmu1a peptide was dissolved in 8 M urea in H_2O (0.2 mM peptide) containing L-glutathione (20 mM, 100 eq) and oxidized L-glutathione (2 mM, 10 eq). The peptide solution was added dropwise onto 50/50 (v/v) ACN/H_2O (0.02 mM final peptide concentration) containing 0.675 M urea, 2.5 M NH_4OAc and adjusted to pH 8 with NH_4OH. The folding solution was agitated for 72 h at 4 °C. After 72 h, the solution was acidified to pH 3–4 with TFA diluted with water and purified by semi-preparative RP-HPLC. The pure fractions were freeze dried and the purity of the peptide was confirmed by analytical RP-HPLC and HRMS analysis.

Analytical RP-HPLC of folding reaction and folded synthetic Pmu1a

Analytical RP-HPLC was run on a Shimadzu LC-20AD (Kyoto, JPN) system using an analytical column (NX-C18 Gemini®, 110 Å, 150 x 2 mm, 5 µm particle size) and a flow rate of 0.5 mL/min. Solvent A was 0.05% TFA in MilliQ water and solvent B was 0.045% TFA in 90% ACN/10% MilliQ water. The separation gradient was from 0–50% B over 50 min and the purification was monitored at 214 and 280 nm.

Mass spectrometry of routine analysis during chemical synthesis and folded synthetic Pmu1a

Solvents used for LC/MS were of HPLC grade. The LC/MS system consisted of an Agilent (Santa Clara, CA, USA) 1200 Series, coupled to an Agilent 6130 quadrupole (electrospray ionization mode, ESI+). Analysis was carried out using an Agilent Poroshell StableBond (2.1 x 75 mm, 5 µm particle size) column and a flow rate of 0.6 mL/min. Solvent A was 0.1% formic acid in MiliQ water and solvent B was 0.1% formic acid in ACN. The gradient was from 0–100% B over 2 min.
Folded peptide was characterized using an Agilent 1200 Series, coupled to Agilent 6520 Accurate-Mass Q-TOF (electrospray ionization mode, ESI+). Analyses were carried out using an Agilent Poroshell StableBond (2.1 x 75 mm, 5 µm particle size) column and a flow rate of 0.6 mL/min.

Solvent A was 0.1% formic acid in MilliQ water and solvent B was 0.1% formic in ACN. The gradient was from 0–100% B over 6 min.

Automated whole-cell patch-clamp electrophysiology

Automated whole-cell patch-clamp recordings were performed on HEK293 cells stably expressing human $Na_V1.4$, 1.6 and 1.7 with β1 (SB Drug Discovery, Glasgow, United Kingdom) with a QPatch II automated electrophysiology platform (Sophion Bioscience, Ballerup, Denmark) using single-hole plates (QPlate 16 with a standard resistance of 2 ± 0.4 MΩ) as previously described[70].
The extracellular solution (ECS) consisted of 145 mM NaCl, 4 mM KCl, 2 mM $CaCl_2$, 1 mM $MgCl_2$, 10 mM HEPES, and 10 mM glucose, pH adjusted to 7.4 with NaOH (adjusted to 305 mOsm/L with sucrose). The intracellular solution (ICS) consisted of (in mM) 140 CsF, 1 EGTA, 5 CsOH, 10 HEPES, and 10 NaCl, pH adjusted to 7.3 with CsOH (adjusted to 320 mOsm/L with sucrose).
Concentration-response curves were acquired using a holding potential of −90 mV and a 50 ms pulse to −20 mV every 20 s (0.05 Hz). Pmu1a was diluted in ECS with 0.1% bovine serum albumin (BSA) and incubated with cells for 160 s at each concentration. Peak current was normalized to buffer control and fitted to a four-parameter Hill equation with variable Hill coefficient.

NMR spectroscopy

NMR spectra were recorded at 290 and 298 K on a Bruker Avance III 600 MHz spectrometer equipped with a cryoprobe (Bruker, Billerica, MA, USA). Sample (≈ 1.2 mg) was dissolved in 90% H_2O/10% D_2O (v/v). D_2O (99.9%) was obtained from Cambridge Isotope Laboratories, Woburn, MA, USA. Two-dimensional spectra including ^1H-^1H TOCSY, ^1H-^1H NOESY, ^1H-^1H DQF-COSY, ^1H-^{15}N HSQC, and ^1H-^{13}C HSQC spectra were recorded using standard Bruker pulse sequences with excitation sculpting for solvent suppression. All spectra were acquired with an interscan delay of 1 s, and NOESY and TOCSY mixing times of 200 ms and 80 ms, respectively, were used. Spectra were referenced to external 4,4-dimethyl-4-silapentane-1-sulfonic acid (DSS; Cambridge Isotope Laboratories) and analyzed using TopSpin v4.1.4 (Bruker, Billerica, MA, USA) and manually assigned using CcpNmr v2.5.2 based on the approach described by Wüthrich [71,72]. The 2D NOESY spectra were automatically assigned, and an ensemble of structures calculated using the program CYANA [73]. Torsion-angle restraints predicted using TALOS-n were used in the structure calculations. The disulfide bond connectivities (Cys2−Cys16, Cys9-Cys21, Cys15-Cys29) were included in the calculations. Structures were visualized using MOLMOL [74].
Slowly exchanging amide protons were detected by recording a time series of one-dimensional and TOCSY spectra immediately following dissolution of lyophilized peptide in D_2O. A combination of preliminary structures and slowly exchanging amide protons was used to predict hydrogen bonds, which were subsequently used in the structure calculations. Structures were visualized using MOLMOL [74]. The coordinates and chemical shifts have been deposited with the PDB code 8FEY and BMRB code 31063, respectively.

Author contributions

SD and EB conceived the project. JG synthesized, folded and purified the toxin Pmu1a with the supervision of CIS. RM, MT and JC performed the whole-cell patch-clamp electrophysiology. JRD

and IV performed the automated whole-cell patch-clamp electrophysiology. DTW and NLD carried out the NMR experiments and determined the structure of Pmu1a. JG wrote the manuscript with the inputs from of all authors. All authors read and approved the final manuscript.

Acknowledgements

The authors would like to thank Guillaume Cazals for technical support (MS and HPLC). HRMS of the synthetic material was performed in the Biophysics Resource, Structural Biophysics Laboratory at NCI Frederick, for which we gratefully acknowledge the assistance of Dr. Sergey Tarasov and Ms. Marzena Dyba. This research was funded by a grant of the French National Research Agency (Labex ICST and ANR-15-CE16-0012 to E.B.; ANR-16-CE34-0002 to S.D.) and was supported [in part] by the Intramural Research Program of the National Cancer Institute, Center for Cancer Research (Grant ZIA BC 012003). I.V. was supported by an Australian NHMRC Career Development Fellowship (APP1162503). J.R.D was support by an Australian Research Council Discovery Early Career Researcher Award (DE210100422). The James Cook University NMR facility was partially funded by the Australian Research Council (N.L.D.) (LE160100218).

Data Availability statement

The coordinates and chemical shifts for the NMR structure of Pmu1a have been deposited to public databases (PDB code 8FEY and BMRB code 31063).

References

1 Cohen SP, Vase L & Hooten WM (2021) Chronic pain: an update on burden, best practices, and new advances. *Lancet* **397**, 2082–2097.

2 Coussens NP, Sittampalam GS, Jonson SG, Hall MD, Gorby HE, Tamiz AP, McManus OB, Felder CC & Rasmussen K (2019) The Opioid Crisis and the Future of Addiction and Pain Therapeutics. *J Pharmacol Exp Ther* **371**, 396–408.

3 Glare P, Aubrey KR & Myles PS (2019) Transition from acute to chronic pain after surgery. *Lancet* **393**, 1537–1546.

4 Lewis RJ & Garcia ML (2003) Therapeutic potential of venom peptides. *Nat Rev Drug Discov* **2**, 790–802.

5 King GF (2011) Venoms as a platform for human drugs: translating toxins into therapeutics. *Expert Opinion on Biological Therapy* **11**, 1469–1484.

6 Casewell NR, Wüster W, Vonk FJ, Harrison RA & Fry BG (2013) Complex cocktails: the evolutionary novelty of venoms. *Trends in Ecology & Evolution* **28**, 219–229.

7 Robinson SD, Undheim EAB, Ueberheide B & King GF (2017) Venom peptides as therapeutics: advances, challenges and the future of venom-peptide discovery. *Expert Rev Proteomics* **14**, 931–939.

8 Wood JN, Boorman JP, Okuse K & Baker MD (2004) Voltage-gated sodium channels and pain pathways. *J Neurobiol* **61**, 55–71.

9 Cox JJ, Reimann F, Nicholas AK, Thornton G, Roberts E, Springell K, Karbani G, Jafri H, Mannan J, Raashid Y, Al-Gazali L, Hamamy H, Valente EM, Gorman S, Williams R, McHale DP, Wood JN, Gribble FM & Woods CG (2006) An SCN9A channelopathy causes congenital inability to experience pain. *Nature* **444**, 894–898.

10 Fertleman CR, Baker MD, Parker KA, Moffatt S, Elmslie FV, Abrahamsen B, Ostman J, Klugbauer N, Wood JN, Gardiner RM & Rees M (2006) SCN9A Mutations in Paroxysmal Extreme Pain Disorder: Allelic Variants Underlie Distinct Channel Defects and Phenotypes. *Neuron* **52**, 767–774.

11 Gonçalves TC, Benoit E, Partiseti M & Servent D (2018) The NaV1.7 Channel Subtype as an Antinociceptive Target for Spider Toxins in Adult Dorsal Root Ganglia Neurons. *Frontiers in Pharmacology* **9**.

12 McArthur JR, Munasinghe NR, Finol-Urdaneta RK, Adams DJ & Christie MJ (2021) Spider Venom Peptide Pn3a Inhibition of Primary Afferent High Voltage-Activated Calcium Channels. *Front Pharmacol* **11**, 633679.

13 McArthur JR, Wen J, Hung A, Finol-Urdaneta RK & Adams DJ (2022) μ-Theraphotoxin-Pn3a inhibition of CaV3.3 channels reveals a novel isoform-selective drug binding site. *Elife* **11**, e74040.

14 Deuis JR, Dekan Z, Wingerd JS, Smith JJ, Munasinghe NR, Bhola RF, Imlach WL, Herzig V, Armstrong DA, Rosengren KJ, Bosmans F, Waxman SG, Dib-Hajj SD, Escoubas P, Minett MS, Christie MJ, King GF, Alewood PF, Lewis RJ, Wood JN & Vetter I (2017) Pharmacological characterisation of the highly NaV1.7 selective spider venom peptide Pn3a. *Sci Rep* **7**.

15 Nicolas S, Zoukimian C, Bosmans F, Montnach J, Diochot S, Cuypers E, De Waard S, Béroud R, Mebs D, Craik D, Boturyn D, Lazdunski M, Tytgat J & De Waard M (2019) Chemical Synthesis, Proper Folding, Nav Channel Selectivity Profile and Analgesic Properties of the Spider Peptide Phlotoxin 1. *Toxins* **11**, 367.

16 Todorovic SM & Jevtovic-Todorovic V (2011) T-type voltage-gated calcium channels as targets for the development of novel pain therapies: T-channels in nociceptive pathways. *British Journal of Pharmacology* **163**, 484–495.

17 Bourinet E, Altier C, Hildebrand ME, Trang T, Salter MW & Zamponi GW (2014) Calcium-Permeable Ion Channels in Pain Signaling. *Physiological Reviews* **94**, 81–140.

18 Miljanich GP (2004) Ziconotide: neuronal calcium channel blocker for treating severe chronic pain. *Curr Med Chem* **11**, 3029–3040.

19 Tranberg CE, Yang A, Vetter I, McArthur JR, Baell JB, Lewis RJ, Tuck KL & Duggan PJ (2012) ω-Conotoxin GVIA Mimetics that Bind and Inhibit Neuronal Cav2.2 Ion Channels. *Marine Drugs* **10**, 2349–2368.

20 Adams DJ, Smith AB, Schroeder CI, Yasuda T & Lewis RJ (2003) ω-Conotoxin CVID Inhibits a Pharmacologically Distinct Voltage-sensitive Calcium Channel Associated with Transmitter Release from Preganglionic Nerve Terminals. *Journal of Biological Chemistry* **278**, 4057–4062.

21 McGivern JG (2007) Ziconotide: a review of its pharmacology and use in the treatment of pain. *Neuropsychiatr Dis Treat* **3**, 69–85.

22 Harding EK & Zamponi GW (2022) Central and peripheral contributions of T-type calcium channels in pain. *Mol Brain* **15**, 39.

23 Todorovic SM & Jevtovic-Todorovic V (2006) The role of T-type calcium channels in peripheral and central pain processing. *CNS Neurol Disord Drug Targets* **5**, 639–653.

24 Perez-Reyes E (2003) Molecular Physiology of Low-Voltage-Activated T-type Calcium Channels. *Physiological Reviews* **83**, 117–161.

25 François A, Laffray S, Pizzoccaro A, Eschalier A & Bourinet E (2014) T-type calcium channels in chronic pain: mouse models and specific blockers. *Pflugers Arch* **466**, 707–717.

26 Todorovic SM, Meyenburg A & Jevtovic-Todorovic V (2002) Mechanical and thermal antinociception in rats following systemic administration of mibefradil, a T-type calcium channel blocker. *Brain Research* **951**, 336–340.

27 Flatters SJL & Bennett GJ (2004) Ethosuximide reverses paclitaxel- and vincristine-induced painful peripheral neuropathy: *Pain* **109**, 150–161.

28 Harding EK, Dedek A, Bonin RP, Salter MW, Snutch TP & Hildebrand ME (2021) The T-type calcium channel antagonist, Z944, reduces spinal excitability and pain hypersensitivity. *Br J Pharmacol* **178**, 3517–3532.

29 Francois A, Kerckhove N, Meleine M, Alloui A, Barrere C, Gelot A, Uebele VN, Renger JJ, Eschalier A, Ardid D & Bourinet E (2013) State-dependent properties of a new T-type calcium channel blocker enhance CaV3.2 selectivity and support analgesic effects. *Pain* **154**, 283–293.

30 Rose KE, Lunardi N, Boscolo A, Dong X, Erisir A, Jevtovic-Todorovic V & Todorovic SM (2013) Immunohistological demonstration of CaV3.2 T-type voltage-gated calcium channel expression in soma of dorsal root ganglion neurons and peripheral axons of rat and mouse. *Neuroscience* **250**, 263–274.

31 François A, Schüetter N, Laffray S, Sanguesa J, Pizzoccaro A, Dubel S, Mantilleri A, Nargeot J, Noël J, Wood JN, Moqrich A, Pongs O & Bourinet E (2015) The Low-Threshold Calcium Channel Cav3.2 Determines Low-Threshold Mechanoreceptor Function. *Cell Reports* **10**, 370–382.

32 Feng X-J, Ma L-X, Jiao C, Kuang H-X, Zeng F, Zhou X-Y, Cheng X-E, Zhu M-Y, Zhang D-Y, Jiang C-Y & Liu T (2019) Nerve injury elevates functional Cav3.2 channels in superficial spinal dorsal horn. *Mol Pain* **15**, 1744806919836569.

33 Bourinet E, Alloui A, Monteil A, Barrère C, Couette B, Poirot O, Pages A, McRory J, Snutch TP, Eschalier A & Nargeot J (2005) Silencing of the Cav3.2 T-type calcium channel gene in sensory neurons demonstrates its major role in nociception. *EMBO J* **24**, 315–324.

34 Marger F, Gelot A, Alloui A, Matricon J, Ferrer JFS, Barrere C, Pizzoccaro A, Muller E, Nargeot J, Snutch TP, Eschalier A, Bourinet E & Ardid D (2011) T-type calcium channels contribute to colonic hypersensitivity in a rat model of irritable bowel syndrome. *Proceedings of the National Academy of Sciences* **108**, 11268–11273.

35 King GF, Gentz MC, Escoubas P & Nicholson GM (2008) A rational nomenclature for naming peptide toxins from spiders and other venomous animals. *Toxicon* **52**, 264–276.

36 King GF, Tedford HW & Maggio F (2002) Structure and function of insecticidal neurotoxins from Australian funnel-web spiders. *Journal of Toxicology: Toxin Reviews* **21**, 361–389.

37 Norton RS & Pallaghy PK (1998) The cystine knot structure of ion channel toxins and related polypeptides. *Toxicon* **36**, 1573–1583.

38 Behrendt R, White P & Offer J (2016) Advances in Fmoc solid-phase peptide synthesis. *Journal of Peptide Science* **22**, 4–27.

39 Jordan JB, Poppe L, Haniu M, Arvedson T, Syed R, Li V, Kohno H, Kim H, Schnier PD, Harvey TS, Miranda LP, Cheetham J & Sasu BJ (2009) Hepcidin revisited, disulfide connectivity, dynamics, and structure. *J Biol Chem* **284**, 24155–24167.

40 Klint JK, Senff S, Rupasinghe DB, Er SY, Herzig V, Nicholson GM & King GF (2012) Spider-venom peptides that target voltage-gated sodium channels: Pharmacological tools and potential therapeutic leads. *Toxicon* **60**, 478–491.

41 Cardoso FC, Castro J, Grundy L, Schober G, Garcia-Caraballo S, Zhao T, Herzig V, King GF, Brierley SM & Lewis RJ (2021) A spider-venom peptide with multitarget activity on sodium and calcium channels alleviates chronic visceral pain in a model of irritable bowel syndrome. *Pain* **162**, 569–581.

42 Dos Santos RG, Van Renterghem C, Martin-Moutot N, Mansuelle P, Cordeiro MN, Diniz CR, Mori Y, De Lima ME & Seagar M (2002) *Phoneutria nigriventer* ω-Phonetoxin IIA Blocks the Ca_v2 Family of Calcium Channels and Interacts with ω-Conotoxin-binding Sites. *J Biol Chem* **277**, 13856–13862.

43 Wang M, Guan X & Liang S (2007) The cross channel activities of spider neurotoxin huwentoxin-I on rat dorsal root ganglion neurons. *Biochemical and Biophysical Research Communications* **357**, 579–583.

44 Liang S, Zhang D, Pan X, Chen Q & Zhou P (1993) Properties and amino acid sequence of huwentoxin-I, a neurotoxin purified from the venom of the Chinese bird spider Selenocosmia Huwena. *Toxicon* **31**, 969–978.

45 Jiang L, Peng L, Chen J, Zhang Y, Xiong X & Liang S (2008) Molecular diversification based on analysis of expressed sequence tags from the venom glands of the Chinese bird spider Ornithoctonus huwena,. *Toxicon* **51**, 1479–1489.

46 Liu Z, Dai J, Dai L, Deng M, Hu Z, Hu W & Liang S (2006) Function and Solution Structure of Huwentoxin-X, a Specific Blocker of N-type Calcium Channels, from the Chinese Bird Spider *Ornithoctonus huwena*. *J Biol Chem* **281**, 8628–8635.

47 Bindokas VP & Adams ME (1989) ?-Aga-I: A presynaptic calcium channel antagonist from venom of the funnel web spider,Agelenopsis aperta. *J Neurobiol* **20**, 171–188.

48 Adams E, Bindokas P & Venema J o-Agatoxins: Novel Calcium Channel Antagonists of Two Subtypes from Funnel Web Spider (Agelenopsis uperta) Venom. , 8.

49 Ertel EA, Warren VA, Adams ME, Griffin PR, Cohen CJ & Smith MM (1994) Type III .omega.-Agatoxins: A Family of Probes for Similar Binding Sites on L- and N-Type Calcium Channels. *Biochemistry* **33**, 5098–5108.

50 Yan L & Adams ME (2000) The Spider Toxin ω-Aga IIIA Defines a High Affinity Site on Neuronal High Voltage-activated Calcium Channels. *J Biol Chem* **275**, 21309–21316.

51 Leão RM, Cruz JS, Diniz CR, Cordeiro MN & Beirão PSL (2000) Inhibition of neuronal high-voltage activated calcium channels by the ω-Phoneutria nigriventer Tx3-3 peptide toxin. *Neuropharmacology* **39**, 1756–1767.

52 Cordeiro M do N, de Figueiredo SG, Valentim A do C, Diniz CR, von Eickstedt VRD, Gilroy J & Richardson M (1993) Purification and amino acid sequences of six Tx3 type neurotoxins from the venom of the Brazilian 'armed' spider Phoneutria Nigriventer (keys.). *Toxicon* **31**, 35–42.

53 Vieira LB, Kushmerick C, Hildebrand ME, Garcia E, Stea A, Cordeiro MN, Richardson M, Gomez MV & Snutch TP (2005) Inhibition of High Voltage-Activated Calcium Channels by Spider Toxin PnTx3-6. *J Pharmacol Exp Ther* **314**, 1370–1377.

54 Vieira LB, Pimenta AMC, Richardson M, Bemquerer MP, Reis HJ, Cruz JS, Gomez MV, Santoro MM, Ferreira-de-Oliveira R, Figueiredo SG, Snutch TP & Cordeiro MN (2007) Leftward Shift in the Voltage-Dependence for Ca2+ Currents Activation Induced by a New Toxin from Phoneutria reidyi (Aranae, Ctenidae) Venom. *Cell Mol Neurobiol* **27**, 129–146.

55 Richardson M, Pimenta AMC, Bemquerer MP, Santoro MM, Beirao PSL, Lima ME, Figueiredo SG, Bloch C, Vasconcelos EAR, Campos FAP, Gomes PC & Cordeiro MN (2006) Comparison of the partial proteomes of the venoms of Brazilian spiders of the genus Phoneutria. *Comparative Biochemistry and Physiology Part C: Toxicology & Pharmacology* **142**, 173–187.

56 Newcomb R, Palma A, Fox J, Gaur S, Lau K, Chung D, Cong R, Bell JR & Horne B (1995) SNX-325, a novel calcium antagonist from the spider Segestria florentina. *Biochemistry* **34**, 8341–8347.

57 Herzig V, Chen Y-C, Chin YK-Y, Dekan Z, Chang Y-W, Yu H-M, Alewood PF, Chen C-C & King GF (2022) The Tarantula Toxin ω-Avsp1a Specifically Inhibits Human CaV3.1 and CaV3.3 via the Extracellular S3-S4 Loop of the Domain 1 Voltage-Sensor. *Biomedicines* **10**, 1066.

58 Gonzales J, Demetrio de Souza Franca P, Jiang Y, Pirovano G, Kossatz S, Guru N, Yarilin D, Agwa AJ, Schroeder CI, Patel S, Ganly I, King GF & Reiner T (2019) Fluorescence Imaging of Peripheral Nerves by a Nav1.7-Targeted Inhibitor Cystine Knot Peptide. *Bioconjugate Chem*, acs.bioconjchem.9b00612.

59 Lim WK, Rösgen J & Englander SW (2009) Urea, but not guanidinium, destabilizes proteins by forming hydrogen bonds to the peptide group. *Proc Natl Acad Sci USA* **106**, 2595–2600.

60 Kim D, Song I, Keum S, Lee T, Jeong M-J, Kim S-S, McEnery MW & Shin H-S (2001) Lack of the Burst Firing of Thalamocortical Relay Neurons and Resistance to Absence Seizures in Mice Lacking α1G T-Type Ca2+ Channels. *Neuron* **31**, 35–45.

61 Choi S, Yu E, Hwang E & Llinás RR (2016) Pathophysiological implication of $Ca_V3.1$ T-type Ca^{2+} channels in trigeminal neuropathic pain. *Proc Natl Acad Sci USA* **113**, 2270–2275.

62 Timic Stamenic T, Feseha S, Valdez R, Zhao W, Klawitter J & Todorovic SM (2019) Alterations in Oscillatory Behavior of Central Medial Thalamic Neurons Demonstrate a Key Role of CaV3.1 Isoform of T-Channels During Isoflurane-Induced Anesthesia. *Cerebral Cortex* **29**, 4679–4696.

63 Sakkaki S, Gangarossa G, Lerat B, Françon D, Forichon L, Chemin J, Valjent E, Lerner-Natoli M & Lory P (2016) Blockade of T-type calcium channels prevents tonic-clonic seizures in a maximal electroshock seizure model. *Neuropharmacology* **101**, 320–329.

64 Astori S, Wimmer RD, Prosser HM, Corti C, Corsi M, Liaudet N, Volterra A, Franken P, Adelman JP & Lüthi A (2011) The Ca(V)3.3 calcium channel is the major sleep spindle pacemaker in thalamus. *Proc Natl Acad Sci U S A* **108**, 13823–13828.

65 Bourinet E & Zamponi GW (2017) Block of voltage-gated calcium channels by peptide toxins. *Neuropharmacology* **127**, 109–115.

66 Rogart RB, Cribbs LL, Muglia LK, Kephart DD & Kaiser MW (1989) Molecular cloning of a putative tetrodotoxin-resistant rat heart Na+ channel isoform. *Proc Natl Acad Sci U S A* **86**, 8170–8174.

67 Caldwell JH, Schaller KL, Lasher RS, Peles E & Levinson SR (2000) Sodium channel Na(v)1.6 is localized at nodes of ranvier, dendrites, and synapses. *Proc Natl Acad Sci U S A* **97**, 5616–5620.

68 Mueller A, Dekan Z, Kaas Q, Agwa AJ, Starobova H, Alewood PF, Schroeder CI, Mobli M, Deuis JR & Vetter I (2020) Mapping the Molecular Surface of the Analgesic $Na_V1.7$-Selective Peptide Pn3a Reveals Residues Essential for Membrane and Channel Interactions. *ACS Pharmacol Transl Sci* **3**, 535–546.

69 Sekiguchi F & Kawabata A (2013) T-type calcium channels: functional regulation and implication in pain signaling. *J Pharmacol Sci* **122**, 244–250.

70 McMahon KL, Tran HNT, Deuis JR, Lewis RJ, Vetter I & Schroeder CI (2020) Discovery, Pharmacological Characterisation and NMR Structure of the Novel μ-Conotoxin SxIIIC, a Potent and Irreversible NaV Channel Inhibitor. *Biomedicines* **8**, E391.

71 Wüthrich K (1986) *NMR of proteins and nucleic acids* Wiley, New York.

72 Vranken WF, Boucher W, Stevens TJ, Fogh RH, Pajon A, Llinas M, Ulrich EL, Markley JL, Ionides J & Laue ED (2005) The CCPN data model for NMR spectroscopy: Development of a software pipeline. *Proteins* **59**, 687–696.

73 Güntert P (2004) Automated NMR Structure Calculation With CYANA. In *Protein NMR Techniques* pp. 353–378. Humana Press, New Jersey.

74 Koradi R, Billeter M & Wüthrich K (1996) MOLMOL: a program for display and analysis of macromolecular structures. *J Mol Graph* **14**, 51–55.

75 Waterhouse AM, Procter JB, Martin DMA, Clamp M & Barton GJ (2009) Jalview Version 2—a multiple sequence alignment editor and analysis workbench. *Bioinformatics* **25**, 1189–1191.

76 Pettersen EF, Goddard TD, Huang CC, Couch GS, Greenblatt DM, Meng EC & Ferrin TE (2004) UCSF Chimera?A visualization system for exploratory research and analysis. *J Comput Chem* **25**, 1605–1612.

Table 1. Summary table of synthetic Pmu1a activity on tested channels.

Channel	IC_{50} or %block ± SEM (n)	Method
$hNa_V1.7$	7.0 ± 0.7 nM (5)	Automated patch clamp
$hNa_V1.7$	5.5 ± 0.4 nM (8)	Manual whole-cell patch clamp
$hNa_V1.6$	9.9 ± 1.7 nM (5)	Automated patch clamp
$hNa_V1.4$	62.9 ± 8.1 nM (5)	Automated patch clamp
$hCa_V3.2$	955.4 ± 235.6 nM (8)	Manual whole-cell patch clamp
	63.5 % ± 4.7 % (6) at 10 μM	
$hCa_V3.1$	95.1 % ± 0.6 % (4) at 10 μM	Manual whole-cell patch clamp
$hCa_V3.3$	90.8 % ± 1.5 % (4) at 10 μM	Manual whole-cell patch clamp

Table 2. Structural statistics for the 20 lowest energy structures of synthetic Pmu1a

Experimental restraints	
Interproton distance restraints	498
Intraresidue	135
Sequential	147
Medium range (i-j < 5)	55
Long range (i-j ≥5)	161
Dihedral-angle restraints	41
RMSD from mean coordinate structure (Å)	
Backbone atoms (residues 4-28)	0.35 ± 0.09
All heavy atoms (residues 4-28)	1.32 ± 0.34
Ramachandran Statistics	
% in most favoured region	76%
% in additionally allowed region	24%

Figure Legends

Figure 1. (A) RP-HPLC chromatogram of crude P. *murinus* venom (1 mg/mL) using a separation gradient from 0–100% B over 100 min. Fraction 32 inhibiting ~80% of $hCa_V3.2$ current is highlighted in red. (B) RP-HPLC trace of fraction 32 using a separation gradient from 20–40% B over 20 min. Sub-fraction 32.6 is highlighted in red. (C) Current trace of sub-fraction 32.6 on HEK293 cells stably overexpressing $hCa_V3.2$ acquired using manual whole cell patch clamp electrophysiology. Currents were elicited by a 180 ms test pulse to −30 mv from a holding potential of −85 mV. (D) RP-HPLC trace and electrospray ionization high-resolution mass spectrometry (ESI-HRMS) spectra of sub-fraction 32.6 using a separation gradient of 0-20% B from 0 to 10 min and 20–40% B from 10 to 30 min.

Figure 2. Sequence alignment between Pmu1a and related sequences Pn3a (P0DM12), GTx1-8-2 (M5AWT1) and GTx1-5-1 (M5AYB3). GTx1-8-2 and GTx1-5-1 are uncharacterized sequences from the spider *Grammostola rosea*, which amino acid sequences show the closest identity to Pmu1a. Conserved residues are highlighted in salmon pink color with conserved cysteine residues in black color. The sequence alignment was generated using Jalview [75].

Figure 3. (A) RP-HPLC chromatograms following thermodynamic folding of Pmu1a in NH_4OAc containing 6 M GnHCl, showing starting material (black trace), and analysis after 72 h of oxidation (blue trace). The product of interest undergoes a shift towards more hydrophobic elution conditions (indicated with an asterisk). (B) HPLC chromatograms showing a time course of thermodynamic folding of Pmu1a peptide in NH_4OAc containing 2.15 M urea, showing starting material (black trace), 24 h (green trace), 48 h (orange trace), and 72 h (blue trace). (C) Thermodynamic folding of Pmu1a in NH_4OAc containing 1.475 M Urea after 72 h of oxidation with 50% ACN (blue trace) and 72 h oxidation without ACN (red trace). (D) RP-HPLC chromatogram and high-resolution mass spectroscopy (HRMS) spectrum of oxidized and purified peptide. The additional peak appears to be a minor conformer most likely arising from dynamic exchange in solution.

Figure 4. (A) Manual whole-cell patch clamp electrophysiology concentration-response curves of Pmu1a on HEK293 cells overexpressing $hCa_V3.2$ (n=8) or CHO cells expressing $hNa_V1.7$ (n=8). The response is normalized to control values. (B) Automated whole-cell patch clamp electrophysiology concentration-response curves of Pmu1a on HEK293 cells overexpressing $hNa_V1.7$ (n=5), $hNa_V1.6$ (n=5), or $hNa_V1.4$ (n=5). The response is normalized to control values. (C) Manual whole-cell patch clamp electrophysiology (currents blockade) of 10 μM Pmu1a on HEK293 cells overexpressing $hCa_V3.2$ (n=6) or $hCa_V3.3$ (n=4) and CHO cells expressing $hCa_V3.1$ (n=4). Currents were elicited at −30 mV from a holding potential of −80 mV at a frequency of 0.2 Hz. (D) Manual whole-cell patch clamp electrophysiology current-voltage curves of 10 μM Pmu1a on HEK293 cells overexpressing $hCa_V3.2$ (n=3) or $hCa_V3.3$ (n=4) and CHO cells expressing $hCa_V3.1$ (n=4). hCa_V3 currents were elicited by a series of step depolarizations (180 ms duration for Cav3.1 and Cav3.2, and 450 ms duration for Cav3.3) ranging from −80 to +50 mV (0.2 Hz) from a holding potential of −90 mV. Current in the presence of Pmu1a were normalized to the current obtained

in the control condition before the peptide application. (E) Effect of 10 µM PmuTx1 on Ca_V3 currents elicited at very positive voltage. Top panel displays the Ca_V3 currents alternatively elicited at −30 mV and at +100 mV (outward current) from a holding potential of −80 mV (test pulse duration 150 ms applied at a frequency of 0.2 Hz). Bottom panel shows the comparison of Pmu1a effects at −30 mV and +100 mV on $Ca_V3.1$ (n=6), $Ca_V3.2$ (n=5) and $Ca_V3.3$ (n=4) current. Data are presented as mean ± SEM.

Figure 5. (A) Stick representation of the 20 lowest-energy structures of Pmu1a. N- and C-termini are labelled and disulfide bonds are highlighted in yellow. (B) Superimposition of Pmu1a (light blue) and Pn3a (dark magenta) over backbone atoms. Residues in Pn3a important for $Na_V1.7$ activity, and their equivalent in Pmu1a, are highlighted in pale green. Residues in Pn3a important for $Na_V1.7$ selectivity over $Na_V1.6$, and their equivalent in Pmu1a, are highlighted in pale red. (C, D) Molecular surface representation of the lowest energy structure of Pmu1a highlighting the amphipathic nature of the peptide with negatively charged residues represented in red, positively charged residues in blue and hydrophobic residues in white. The final structures were visualized using UCSF Chimera [76].

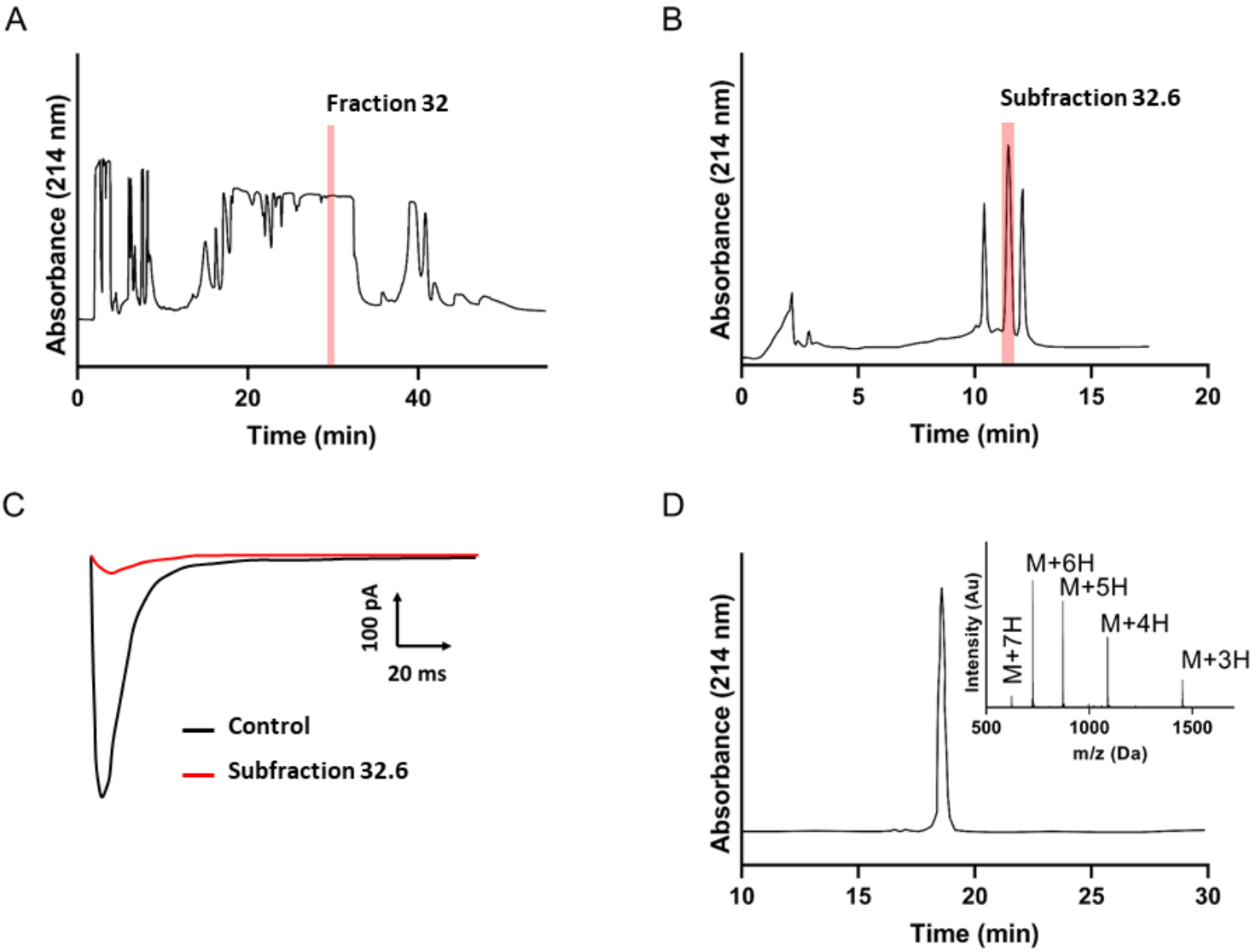

FEBS_16773_Figure 1.tif

FEBS_16773_Figure 2.tif

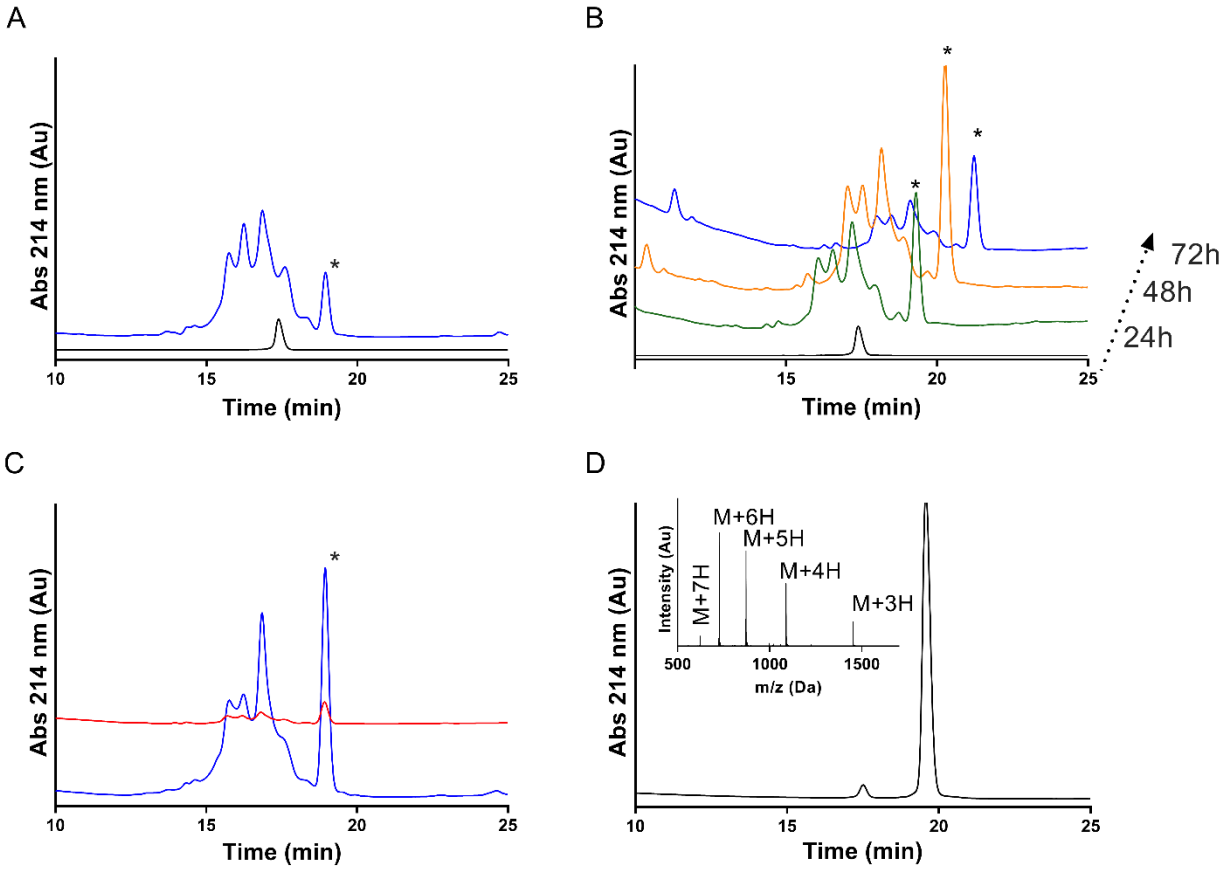

FEBS_16773_Figure 3.tif

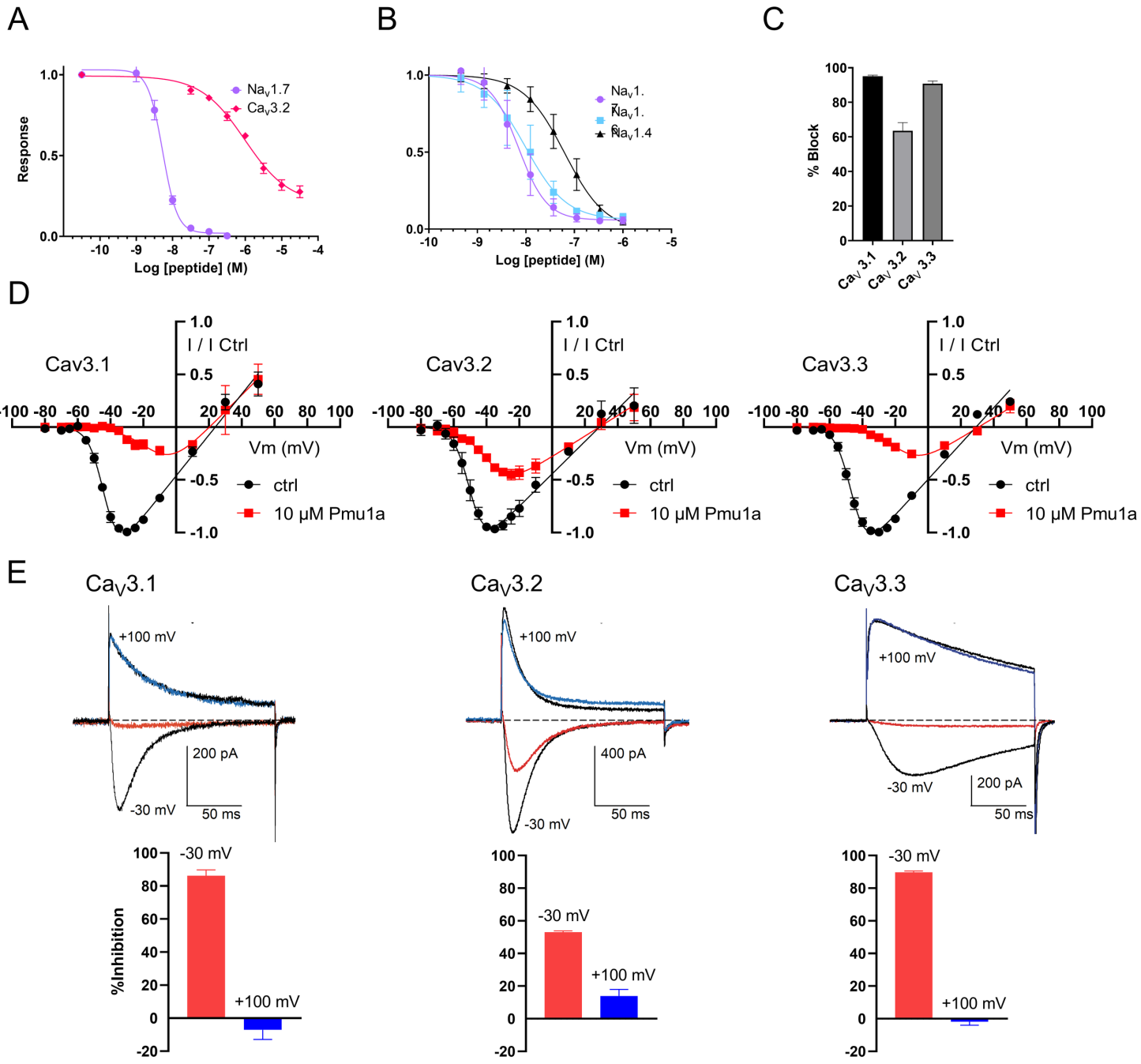

FEBS_16773_Figure4.tif

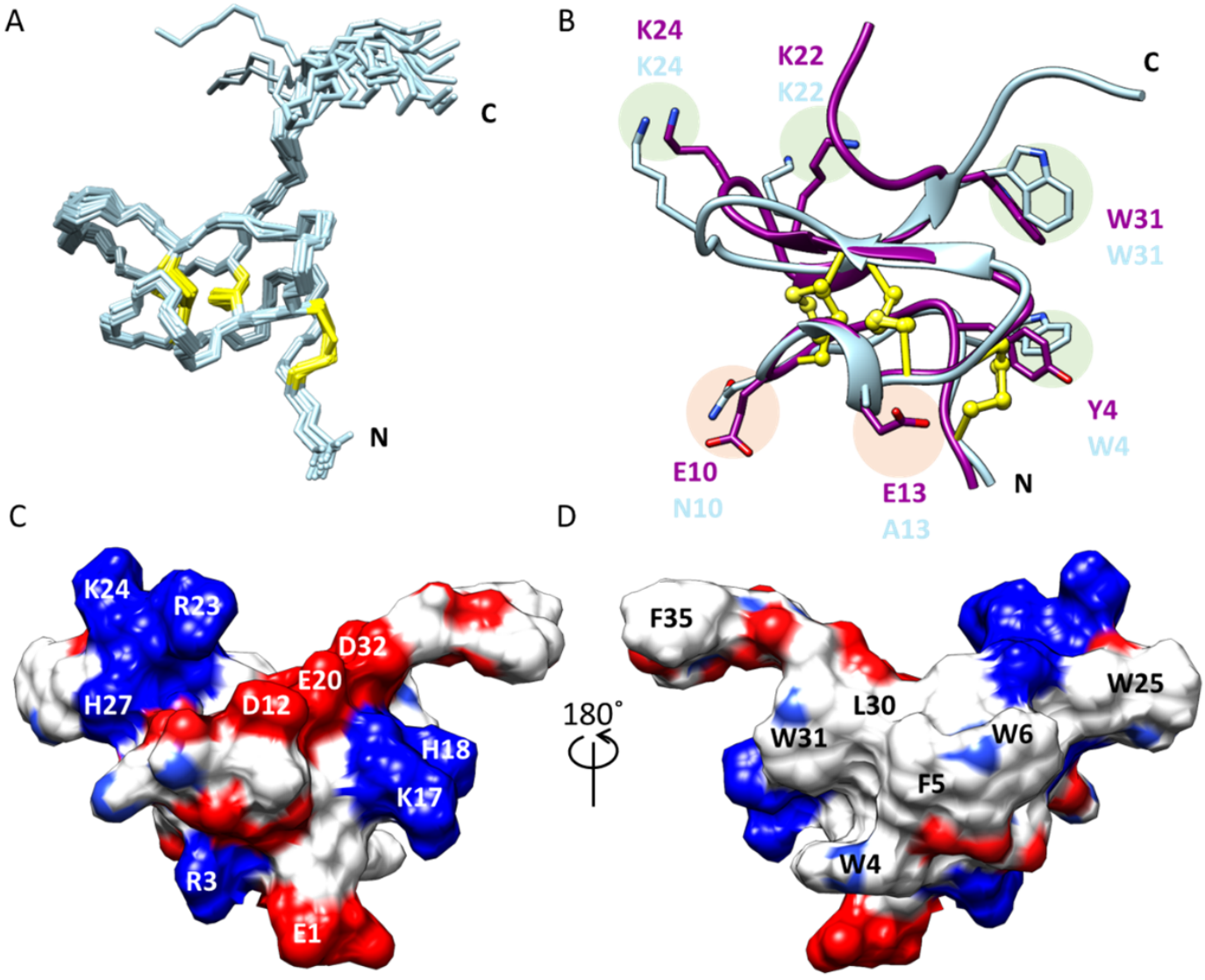

FEBS_16773_Figure 5.tif